JOURNAL OF GEOPHYSICAL RESEARCH, VOL. 99, NO. D6, PAGES 12,793–12,808, JUNE 20, 1994

Influence of plumes from biomass burning on atmospheric chemistry over the equatorial and tropical South Atlantic during CITE 3

M. O. Andreae,[1] B. E. Anderson,[2] D. R. Blake,[3] J. D. Bradshaw,[4]
J. E. Collins,[2] G. L. Gregory,[2] G. W. Sachse,[2] and M. C. Shipham[2]

Abstract. During all eight flights conducted over the equatorial and tropical South Atlantic (27°–35°W, 2°N–11°S; September 9–22, 1989) in the course of the Chemical Instrumentation Test and Evaluation (CITE 3) experiment, we observed haze layers with elevated concentrations of aerosols, O_3, CO, and other trace gases related to biomass burning emissions. They occurred at altitudes between 1000 and 5200 m and were usually only some 100–300 m thick. These layers extended horizontally over several 100 km and were marked by the presence of visible brownish haze. These layers strongly influenced the chemical characteristics of the atmosphere over this remote oceanic region. Air mass trajectories indicate that these layers originate in the biomass burning regions of Africa and South America and typically have aged at least 10 days since the time of emission. In the haze layers, O_3 and CO concentrations up to 90 and 210 ppb were observed, respectively. The two species were highly correlated. The ratio $\Delta O_3/\Delta CO$ (Δ, concentrations in plume minus background concentrations) is typically in the range 0.2–0.7, much higher than the ratios in the less aged plumes investigated previously in Amazonia. In most cases, aerosol (0.12–3 μm diameter) number concentrations were also elevated by up to 400 cm^{-3} in the layers; aerosol enrichments were also strongly correlated with elevated CO levels. Clear correlations between CO and NO_x enrichments were not apparent due to the age of the plumes, in which most NO_x would have already reacted away within 1–2 days. Only in some of the plumes could clear correlations between NO_y and CO be identified; the absence of a general correlation between NO_y and CO may be due to instrumental limitations and to variable sinks for NO_y. The average enrichment of $\Delta NO_y/\Delta CO$ was quite high, consistent with the efficient production of ozone observed in the plumes. The chemical characteristics of the haze layers, together with remote sensing information and trajectory calculations, suggest that fire emissions (in Africa and/or South America) are the primary source of the haze layer components.

Introduction

Satellite studies have shown high levels of ozone in the troposphere over the tropical and equatorial South Atlantic [*Fishman and Larsen*, 1987; *Fishman et al.*, 1990, 1991]. Ozone soundings made at Natal on the east coast of Brazil also show the presence of layers with elevated ozone concentrations in the middle and upper troposphere [*Kirchhoff and Nobre*, 1986; *Kirchhoff et al.*, 1990, 1991]. At Ascension Island, in the center of the tropical South Atlantic, the same enhancement of ozone in the middle and upper troposphere has been observed [*Cros et al.*, 1992]. This phenomenon is most pronounced during the southern hemisphere dry season in South America and Africa, when burning of savannas and tropical forests is widespread. Since the ozone-laden air masses over the South Atlantic have passed over the African and South American continents, it has been proposed that the formation of ozone is due to photochemical reactions in the plumes from biomass burning in the African and South American tropics [*Kirchhoff and Nobre*, 1986; *Fishman et al.*, 1990; *Watson et al.*, 1990]. This view is supported by the observation of high concentrations of CO in the middle and upper troposphere over Southern Africa, South America, and the South Atlantic made by the space-borne MAPS instrument in November 1981 and October 1984 [*Reichle et al.*, 1986, 1990].

The second part of the Chemical Instrumentation Test and Evaluation (CITE 3) expedition [*Hoell et al.*, 1993] took place over the tropical and equatorial Atlantic in September 1989. The main objective of the CITE 3 experiment was an intercomparison of various instruments to measure atmospheric sulfur species, but instruments to measure O_3, CO, nitrogen oxides, and various aerosol characteristics were also present on the research aircraft. This provided an opportunity to conduct the first in situ measurements in biomass burning plumes over the South Atlantic. Similar measurements had been conducted previously much closer to the source regions in South America

[1]Max Planck Institute for Chemistry, Biogeochemistry Department, Mainz, Germany.
[2]NASA Langley Research Center, Atmospheric Sciences Division, Hampton, Virginia.
[3]Department of Chemistry, University of California, Irvine.
[4]Georgia Institute of Technology, School of Geophysical Sciences, Atlanta, Georgia.

Paper number 94JD00263.
0148-0227/94/94JD-00263$05.00

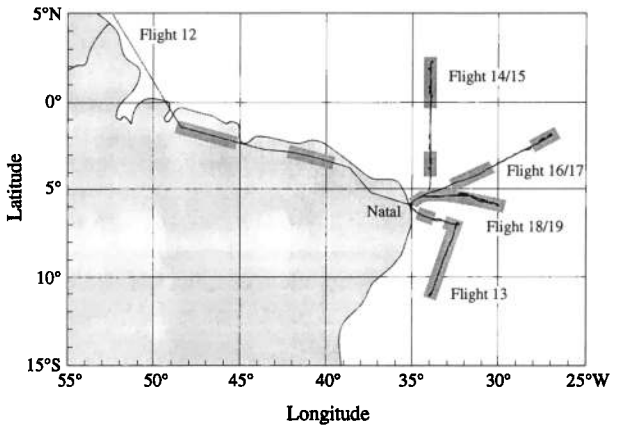

Figure 1. Map of the study area. Flight tracks are indicated by solid lines; the shaded areas along the flight tracks indicate the regions where evidence for haze layers from biomass burning was observed. Flights 14 and 15, 16 and 17, 18 and 19 were conducted in pairs, following the same tracks.

[*Crutzen et al.*, 1985; *Andreae et al.*, 1988; *Kaufman et al.*, 1992] and Africa [*Andreae et al.*, 1992; *Marenco et al.*, 1990]. Ozone sondes were launched at Natal, on the coast of Brazil, simultaneously with the CITE 3 aircraft investigations. This provided an opportunity to observe the presence of additional ozone-enriched layers above the altitudes accessible to the research aircraft [*Hoell et al.*, 1993].

In this paper we present the results of our airborne measurements of trace gases and aerosols in tropospheric haze layers over the equatorial and tropical South Atlantic. We use air mass trajectories and other meteorological data to determine the origin of these haze layers.

Methods

In situ measurements (ozone, carbon monoxide, nitrogen oxides, and aerosol particles) and grab sampling (nonmethane hydrocarbons (NMHC)) were conducted on the NASA Electra research aircraft, which was based at Natal, Brazil, for the second half of the CITE 3 experiment (September 9–22, 1989). The research flights took place in the region between longitude 27° and 35°W and latitude 2°N and 11°S. Data from the transit flight to Natal (flight 12) also showed evidence of plumes from biomass burning in the region from 50° to 35°W and will therefore be included in this paper. The tracks of flights 12–19 are shown in Figure 1; the shaded areas along the flight tracks indicate the regions where our measurements indicated the presence of elevated amounts of O_3, CO, and aerosol from biomass burning.

The sampling and analytical methods employed for the collection of data on the haze layers are described in detail in other publications by the members of the CITE 3 science team; therefore they will be outlined only briefly in the following paragraphs.

Ozone

Ozone concentrations were determined using a C_2H_4 chemiluminescence instrument which had been modified to compensate for altitude variations [*Gregory et al.*, 1983]. The instrument was calibrated using the NO gas phase titration technique with National Institute for Standards and Technology (formerly National Bureau of Standards) traceable calibration gases. It has a response time of about 2 s to 90% of reading, a precision of 2 ppb or 2% (whichever is largest) for a 10-s average, and an absolute accuracy of 5 ppb or 5%. Sample air was delivered to the instrument via a Teflon-lined inlet which extended about 30 cm out from the aircraft skin into relatively undisturbed airflow. Data were recorded at 1-s intervals; 10-s averages were used for the profiles and analyses presented in this paper.

Carbon Monoxide

CO measurements were provided by the differential absorption CO measurement (DACOM), a diode-laser-based instrument designed to measure CO aboard an aircraft platform. The instrument determines CO by modulating the laser wavelength across an isolated absorption line in the 4.7-μm band and then detecting the periodic attenuation experienced by the laser beam due to the absorption by CO molecules in the White cell. The pressure in the White cell is maintained at 50 torr to narrow the CO absorption line and other potentially interfering absorption lines. An inlet probe is extended past the slipstream of the aircraft to capture the sample air, which is then passed through a chemical dryer to remove H_2O vapor by reaction with $Mg(ClO_4)$. The sample air then enters the pressure-controlled sample cell which contains a 12.5-m folded optical path and then is continuously pumped overboard. Approximately 20% of the diode laser power is directed to a wavelength stabilization leg which provides an error signal when the laser wavelength sweep drifts from the CO absorption line center. The instrument is calibrated approximately every 15 min by passing a calibration gas of known CO concentration through the sample system. Precision and accuracy are improved by interpolating between these frequent calibrations. Power fluctuations are removed by dividing the differential absorption signal by the transmitted power from the laser, which can be measured using an optical chopper and a lock-in amplifier.

Nitrogen Oxides

Nitric oxide, NO_2, and NO_y were measured simultaneously with the Georgia Tech two-photon/laser-induced fluorescence (TP/LIF) instrument [*Bradshaw et al.*, 1985; *Sandholm et al.*, 1990]. This spectroscopically selective NO technique was used to simultaneously determine NO, NO produced from the photolysis of NO_2, and NO produced from the reduction of NO_y compounds using a 300°C gold catalytic surface with 0.3% CO as a reducing agent. A 1-kW photolytic converter was operated with a photolysis passband of 350 nm $< \lambda <$ 410 nm, a photolytic yield ranging from 30 to 60%, and sample residence times ranging from 2 to 4.5 s. A porcelain-glass-coated inlet was used to sample ambient air in an orientation perpendicular to the airstream. These N_xO_y measurements were reported using an integration time of 180 s. Accuracy of the instrument calibration is estimated to be ±16% for NO and ±18% for NO_2 and NO_y at the 95% confidence limit. Limits of detection for a 180-s signal integration were ~3 ppt for NO and ~10 ppt for NO_2 with a signal-to-noise ratio of 2:1. The typical measurement precision for NO_y (at 95% confidence limit) was approximately ±10% at 500 ppt increasing to approximately ±20% at 200 ppt [*Sandholm et al.*, 1990, 1992]. The NO_y measurements included some fractional component of fine particulate nitrate-containing aerosols. The plume layers generated

a memory effect in the unheated portion of the NO_y sampling line. Measurements adversely affected by this phenomenon were not included in the analysis of the data.

Aerosols

Aerosol densities as a function of time and size diameter were measured with two optical scattering probes mounted externally to the aircraft. Both probes were manufactured and calibrated by particle measuring systems (Boulder, Colorado). An active scattering aerosol spectrometer probe (ASASP) was used to monitor 0.12- to 3.1-μm-diameter particles, while a forward scattering spectrometer probe (FSSP) was used for the 0.5- to 8.0-μm range. According to the manufacturer's specifications, the ASASP, or "small" aerosol probe, classifies particles into 15 size bins of progressively increasing width: bin 1 is 0.025 μm wide, bin 2 is 0.050 μm wide, and bin 3 is 0.075 μm wide. The FSSP, or "large" aerosol probe, also provides 15 channels of information, but it sizes particles into 0.5-μm wide bins. In both probes the relative humidity inside the measurement cavity is close to the ambient value. Profile and size distribution plots were prepared from 10- and 60-s averaged data, respectively. In the case of the size distribution plots, ASASP data were used for the 0.12 to 0.5 μm range while FSSP data filled the 0.5- to 8.0-μm range.

Nonmethane Hydrocarbons

The analytical details for the determination of nonmethane hydrocarbons were described in detail by *Blake et al.* [1992]. Samples for the determination of nonmethane hydrocarbons were collected in specially manufactured and cleaned stainless steel canisters. The air sample in the canister was compressed to a pressure of 2.7 bar using a metal-bellows pump. Samples were analyzed by gas chromatography within 4–7 days after collection. A dried air sample from Niwot ridge was used as a secondary standard for daily calibrations. This sample had been calibrated against artificially prepared reference standard mixtures. The accuracy of the determinations was about 5%.

Meteorological Products

A variety of meteorological products, including GOES and METEOSAT satellite imagery, isentropic back trajectory analysis, streamline and wind vector fields, and soundings, were used to describe salient meteorological features observed during CITE 3. The trajectory analysis procedure was developed by *Danielsen* [1961] and further refined by *Haagensen and Shapiro* [1979]. The package inputs both NMC (National Meteorological Center) derived fields and soundings and was used to generate 7- to 10-day back trajectories for this and other papers.

Results and Discussion

Meteorological Overview

The meteorological environment during the CITE 3 experiment is discussed in detail by *Shipham et al.* [1993]; only a brief overview will be presented here. The dominant synoptic feature over the South Atlantic Ocean during the study period (September 9–22, 1989) was the South Atlantic subtropical anticyclone, which generally transported air across the tropical Atlantic toward eastern Brazil. In the lower troposphere (850 hPa, ~1.5 km), the mean axis of the South Atlantic subtropical anticyclone was located between 18° and 26°S latitude, while in the middle troposphere (700–500 hPa, ~3–6 km) the mean ridge axis was situated farther north, between 12° and 20°S latitude. Pronounced subsidence along the northern periphery of the South Atlantic subtropical anticyclone contributed to the well-defined trade wind inversion and the highly stratified nature of the atmosphere which was frequently observed over the study area.

With this circulation regime a prevailing deep easterly to southeasterly trade wind flow was present in the vicinity of Natal, with a long low-level fetch over the tropical South Atlantic. A westerly flow off the South American continent dominated south of the ridge axis. Some high-altitude recirculation of air from South America was observed, as was cross-equatorial transport which had come from northern Africa.

Variations in the relative positions and intensities of circulation features over South America, Africa, and the South Atlantic basin led to pronounced differences between the transport pathways of air sampled during the seven Natal flights. Intense midlatitude cyclones propagating eastward across the South Atlantic perturbed the location and strength of individual subtropical anticyclone centers. Disturbances also moved westward across the tropical Atlantic, initiating episodes of cross-equatorial flow from Africa.

Air Mass Origin and Transport

As discussed in detail below, haze layers originating from biomass burning plumes were identified during flights 12–19 based on elevated levels of aerosol particles, CO, O_3, and other trace gases. In the following paragraphs we will describe the origin and transport paths of these smoke-laden air masses using some typical examples. The first such layer was encountered during the second half of flight 12, the transit flight from Barbados to Natal (Figure 2). The occurrence of elevated concentrations of pyrogenic chemical species coincides exactly

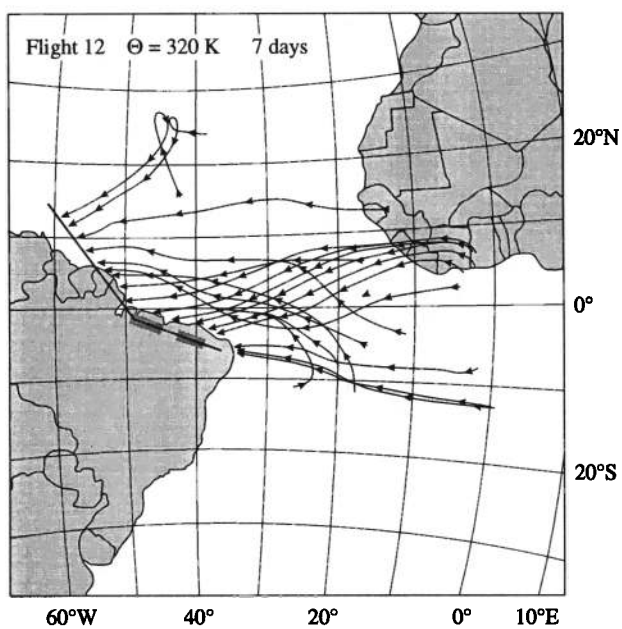

Figure 2. Seven-day air mass back trajectories for flight 12 (Barbados to Natal; trajectories end at 0000 UT, September 11, 1989). The sections of the track where smoke plumes were encountered are marked by a shaded background.

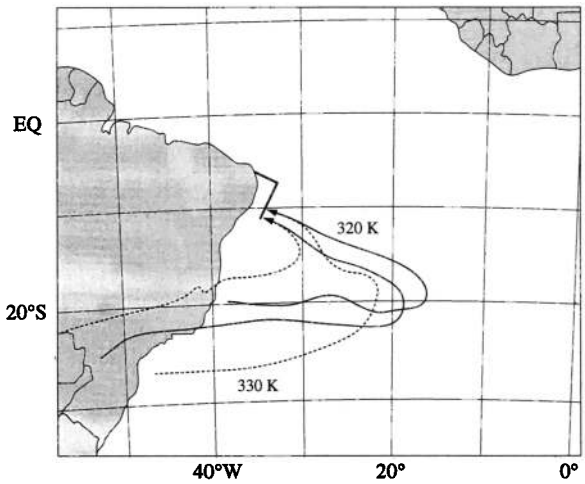

Figure 3. Seven-day air mass back trajectories for the upper altitude levels of profile 13A, flight 13 (trajectories end at 1200 UT, September 12, 1989).

with the flight segments during which the air mass trajectories originate in West Africa, suggesting that the input of smoke into this air mass occurred in northern Africa, possibly West Africa, at least 6–7 days prior to sampling.

Flight 13 provides the clearest case for the impact of biomass burning in South America on the study region. High-level (320–330 K) trajectories (Figure 3) show a counterclockwise recirculation from the southern Brazil/Paraguay region, where fires in the grasslands and savannas are known to occur at this time of year [*Andreae*, 1993b]. Deforestation fires at the southern rim of the Amazon forest also reach their maximum at this time of year [*Kirchhoff et al.*, 1989] and may have contributed to the pyrogenic pollutants in this air mass. Air sampled on flight 13 at altitudes above 3 km had some of the highest O_3/CO ratios of the whole expedition (Figure 4) and appeared to be a mixture of high-altitude plumes and upper tropospheric air.

Air mass origins in South America (southern Brazil, Uruguay, and Argentina) are also suggested by the trajectories for some of the plumes sampled during flights 18 and 19 (Figure 5; September 22/23, 1989). This applies particularly to the altitude range up to ~2.5 km, below the trade wind inversion, where the air had been slowly recirculating around the subtropical anticyclone.

Most of the haze plumes, however, appear to originate in Africa. The 10-day trajectories originate predominantly in two regions: West Africa, particularly Liberia and Ivory Coast (Figure 6, flights 12, 14, and 15), and in a band from

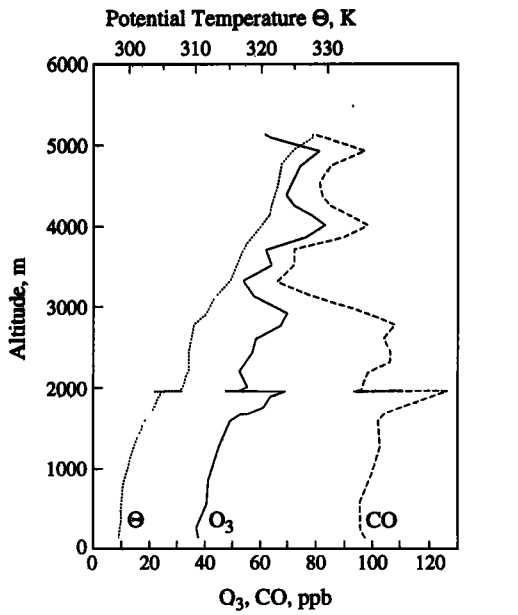

Figure 4. Vertical profile of ozone, CO, and potential temperature Θ for profile 13A (flight 13, 1549–1602 UT). The discontinuity at 2000 m altitude is due to a level flight segment between the upper and the lower parts of the profile.

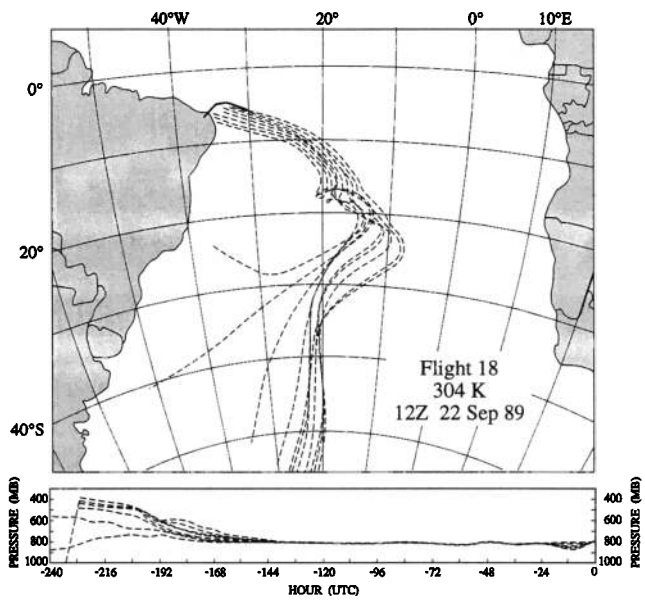

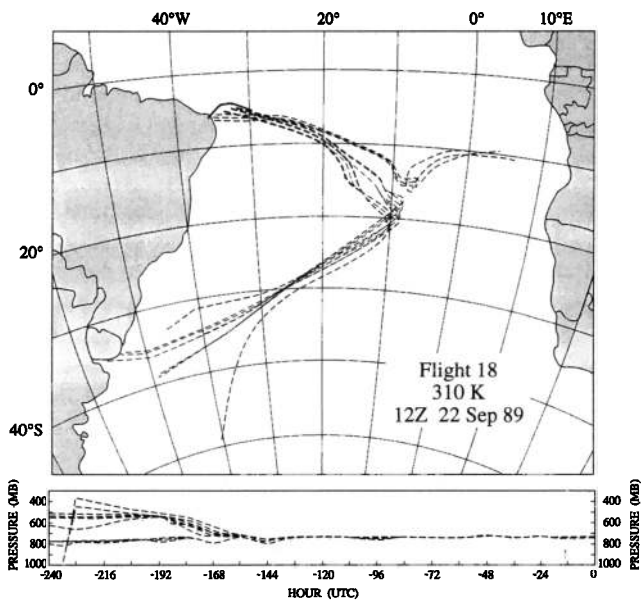

Figure 5. Ten-day air mass back trajectories for plumes sampled on flights 18, showing recirculation of air masses from South America around the subtropical anticyclone.

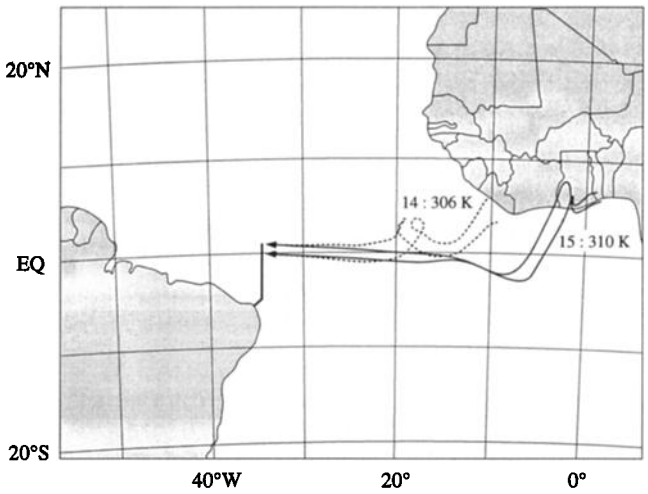

Figure 6. Ten-day air mass back trajectories for plumes sampled on flights 14 and 15, showing air mass origins in West Africa. The dotted curves represent the trajectories for flight 14 at 306 K; the solid curves are for flight 15 at 310 K.

the Congo south through Zaire into Angola (Figure 7, flights 16, 17, and 18). It must be emphasized that this is at best an indication of where these air masses have left the African continent; the input of smoke could have happened considerably earlier and in a different region. Recent investigations of air mass transport in southern Africa show that smoke from fires in the savanna belt reaching from Angola through Zambia and Zaire to Tanzania often is recirculated for some time over the African continent, before being ejected over the Atlantic Ocean along the coast of Angola and Zaire.

Finally, many of the 10-day trajectories originate over the South Atlantic, usually the region west of the coast of South Africa, Namibia, and Angola (Figure 8, flights 13, 14, 15, and 16). This is typically the case for plumes which were

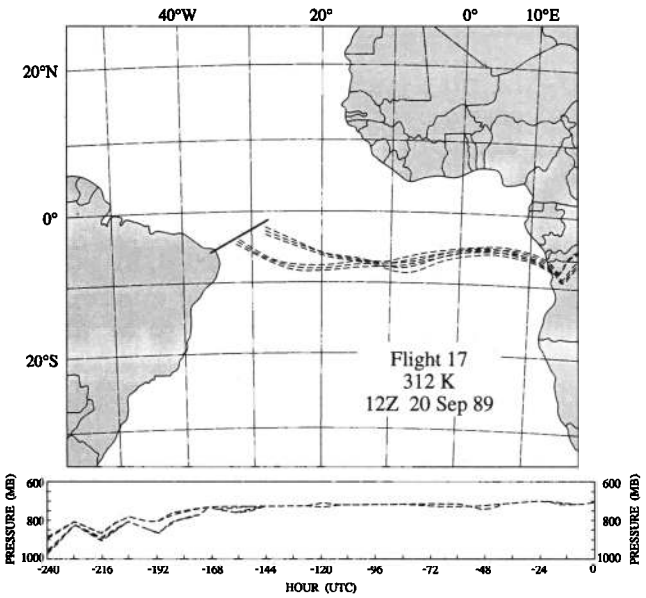

Figure 7. Ten-day air mass back trajectories for plumes sampled on flight 17 above the trade wind inversion, showing air mass origins in tropical southern Africa.

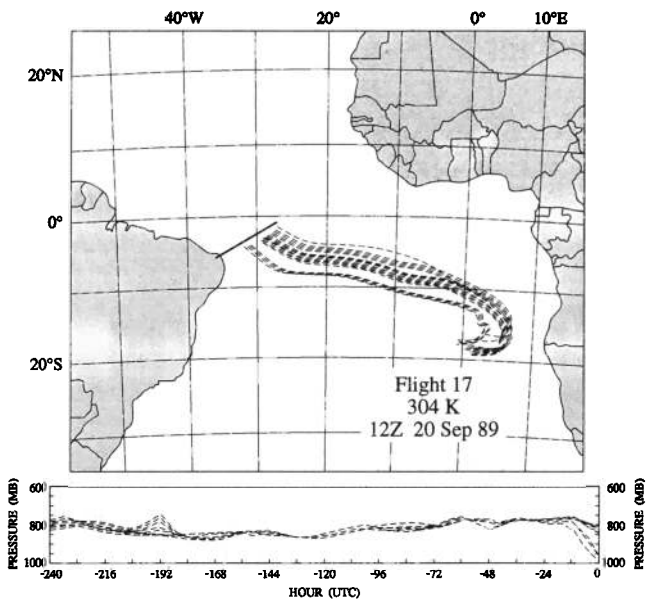

Figure 8. Ten-day air mass back trajectories for plumes sampled on flight 16 in the boundary layer. Air masses can only be traced back to a region over the South Atlantic off southern Africa.

encountered below the trade wind inversion, at potential temperatures of 302–308 K. A good example is flight 16, where the entire boundary layer appeared polluted, with numerous plumes observed at potential temperatures of 302–306 K, corresponding to altitudes below 2 km (Figure 8). Streamline analysis [*Shipham et al.*, 1993] suggests that these air masses may have originated in southern Africa.

Visual Observations

Visible haze layers were present on all flights in the study region, with the obvious exception of flights 15 and 17, which were conducted at night. The color of these layers ranged from almost pure white to brown (Figure 9). They could be seen throughout a wide range of altitudes, from about 1 km to above 5.2 km, the highest level reached by the aircraft. They were most frequent just above the tops of the trade wind cumulus, in the altitude range from 1.5 to 3 km. Seen from the side, the layers appeared quite thin, frequently with sharp edges above and below, and seemed to extend to the horizon. Individual layers could often be traced over some tens of kilometers during horizontal flight legs. The chemical fine structure of the layers, which is evident in the CO, O_3, and aerosol soundings discussed below as a series of multiple peaks, is seen as multiple layers when viewed from the side.

Ozone and Carbon Monoxide

From the chemical measurements the presence of the biomass-burning-derived plumes was most clearly evident in the closely correlated peaks of O_3 and CO concentrations observed during soundings obtained during climbs or descents of the aircraft. In the course of the study period we identified 34 cases where haze layers were penetrated during soundings, sometimes with several sublayers present within one major layer. Figure 10 shows a number of representative examples of this type of data. In agreement with the visual

Figure 9. Haze layers, as seen from the NASA Electra aircraft during flight 14 on September 15, 1989 (a) near 5°S and 34°W at an altitude of 2 km and (b) near 1°N and 34°W at an altitude of 1.5 km.

observations discussed above, we find O_3 and CO enriched in discrete layers with a thickness of about 300–1000 m. The maximum concentrations in these layers are in the case of CO some 50–120 ppb, and in the case of O_3 some 20–40 ppb higher than the background concentrations measured at the same altitudes outside of the plumes. The enhancement of O_3 and CO in the lower marine troposphere observed during CITE 3 is even more dramatic, when the measurements are compared with data obtained in the same region outside of the burning season, e.g., the CO and O_3 profiles obtained over the Atlantic at about 1°S during ABLE 2A [*Sachse et al.*, 1988; *Gregory et al.*, 1988] and the O_3 profiles from the December to May period at Natal [*Kirchhoff and Nobre*, 1986; *Kirchhoff et al.*, 1991]. These studies show that CO background levels in this region are about 65–80 ppb and O_3 background levels about 15–20 ppb at the surface, increasing to about 40 ppb at 5 km. The resulting enhancements are then 65–145 ppb CO and 35–65 ppb O_3. Even outside of the plumes, CO levels are some 20–40 ppb above the background level from the surface to about 3 km altitude, suggesting that convective activity has distributed combustion-derived material throughout the planetary boundary layer.

In addition to the vertical profiles discussed above, measurements on the plumes were also made during horizontal flight legs. A total of 15 horizontal flight segments were conducted within the haze layers. Figure 11 shows some examples of the type of data obtained. Again, we find CO and O_3 to be highly correlated. To quantify the observed correlation between O_3 and CO, we have performed regression analyses on our data. Here, we have used the same procedure as we have applied previously in our study on haze layers over the Amazon basin [*Andreae et al.*, 1988]. In this analysis, it is assumed that the air in the plume mixes with the air above and below. The chemical composition of the plume can then be characterized by the regression slope of O_3 versus CO, the "ozone production ratio" ($\Delta O_3/\Delta CO$), which represents the number of O_3 molecules formed in the plume per molecule of CO emitted in the combustion process (assuming that only a negligible amount of CO has been photooxidized during transport). To correct for the gradual increase of O_3 concentration with height in the background atmosphere, a line is fitted to the background, and the background values are subtracted from the ambient concentrations. Where appropriate, an analogous correction is performed on the CO profile. No such correction is necessary for the data from level flight legs.

The results of this analysis are summarized in Table 1. The degree of correlation is quite high ($r^2 > 0.7$) in most cases. The mean value of $\Delta O_3/\Delta CO$ for all cases is 0.46 ± 0.23 ($n = 40$). This value is similar to the ratio observed during the first part of CITE 3 in the North American plume (0.4, with a range of 0.17–0.42 [*Anderson et al.*, 1993a]) but much higher than previously observed in biomass burning plumes. In the haze layers over Amazonia we found a $\Delta O_3/\Delta CO$ ratio of 0.044 ± 0.030 [*Andreae et al.*, 1988], over the Brazilian savanna *Greenberg et al.* [1984] measured 0.056, and in the plumes over the northern Congo the ratio was 0.14 [*Andreae*

Figure 9. (continued)

et al., 1992]. In measurements of plumes from wildfires in the Arctic tundra, *Wofsy et al.* [1992] also observed low $\Delta O_3/\Delta CO$ ratios (0.095 ± 0.060). The difference between the relative amounts in O_3 production in these plumes may be attributable to two main factors, plume age and the NO_x/CO ratio in the fire emissions. The model study of *Chatfield and Delany* [1990] shows that O_3 concentrations in diluted smoke from biomass burning in the midtroposphere keeps increasing over 14 days, while the CO concentration remains almost constant. The plumes investigated here have been in the atmosphere for at least 7 days in the case of the plumes recycled from South America, but in most cases they have been exposed to photochemical processing for over 10 days. In contrast, the transport times of the plumes we sampled in Amazonia was of the order of 1 day, and those sampled in the northern Congo were about 4 days old. An equally important factor, however, may be the NO_x/CO ratio in the emissions. In fact, *Jacob et al.* [1992] have suggested that the NO_x/NMHC ratio in the emissions is likely to be the controlling factor in the photochemical production of O_3 in the plumes and that for typical NMHC/CO ratios, $\Delta NO_x/\Delta CO$ emission ratios of the order of 0.1 or greater are required to lead to the levels of O_3 production observed here. This issue will be discussed in more detail in the section on nitrogen oxides.

Aerosols

Aerosol particles were also found to be enriched in the plumes, consistent with the presence of visible haze. The enrichment is most clearly seen in the data from the ASASP probe, which determines particles in the 0.12- to 3.1-μm diameter range. The sum of the particles present in this size range, N_p, is plotted together with the O_3 and CO data in Figures 10 and 11. These figures clearly show the high degree of coherence between aerosol count and O_3 and CO concentrations in the plumes. This is further borne out by the results of the regression analyses (Table 1; the data have been corrected for sampling altitude by converting the aerosol concentrations to standard temperature and pressure). A very consistent ratio of $\Delta N_p/\Delta CO$ is observed, with an average value of 5.2 ± 1.7 cm^{-3} (STP) ppb^{-1} (based on 37 observed cases).

Number/size and mass/size spectra from the haze layers show that the number concentrations peak near the lower end of the size range detected by the ASASP probe, while the peak in the mass/size distribution lies near 0.3 μm, well within the range of the ASASP probe (Figure 12). For comparison, a size spectrum obtained with a similar instrument directly above a savanna fire in South Africa is also shown in Figure 12. A close agreement is seen between the fresh smoke and the aged haze aerosols sampled during CITE 3. Mass median diameters in fresh fire plumes are typically in the range of 0.1–0.3 μm and evolve toward values in the range of 0.2–0.4 μm during the first few hours after emission [*Radke et al.*, 1978, 1988, 1991; *Stith et al.*, 1981; *Holben et al.*, 1991]. It appears therefore that continued aging of the aerosols over 4 days to 2 weeks, as must be assumed for the CITE 3 plumes, did not have a major additional effect on aerosol size distributions. A second mass peak was frequently seen in the plumes at diameters of

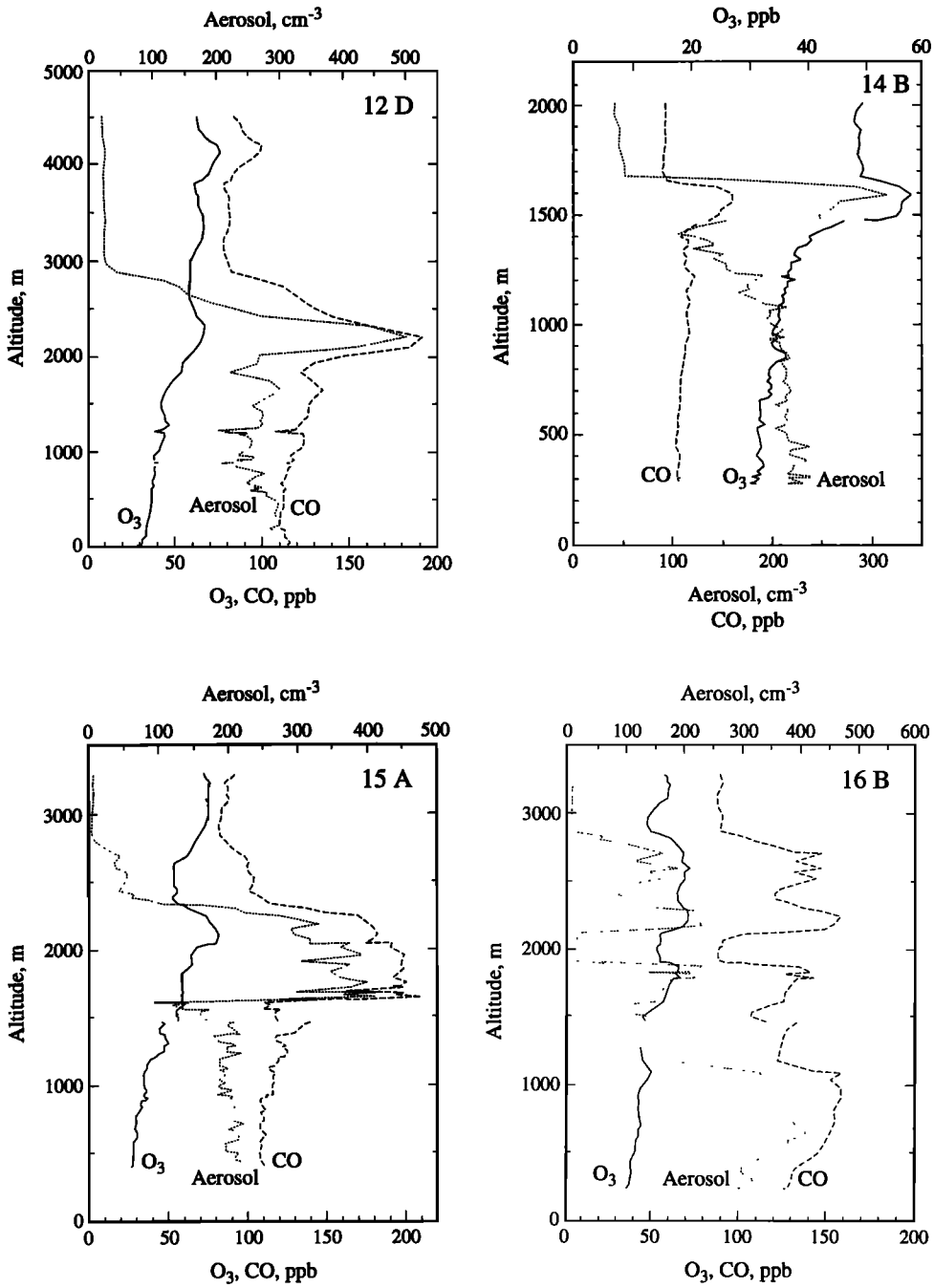

Figure 10. Vertical profiles of O_3, CO, and fine aerosol particle concentration over the Atlantic Ocean (data from profiles 12D, 14B, 15A, 16B, 17A, 18B).

several micrometers. The presence of a mode in a similar size range is also evident in the measurements over the fresh savanna fires and may be related to entrainment of soil and ash particles due to the turbulence created by the flames. Entrainment of sea-salt aerosols during convective events over the ocean may also have contributed to this mode.

Since particles smaller than 0.12 μm, which are not detected by the ASASP, are also expected to be present, we compared the results from the ASASP probe with the available data on total particle (condensation nucleus (CN)) concentrations as determined with a TSI 3020 Aitken nuclei counter (R. J. Ferek, personal communication, 1989). The ratio between ASASP counts and CN counts, N_p/N_{CN}, ranges from 0.024 to 1.23 and depends strongly on relative humidity (Figure 13). At the lowest humidities observed in the haze layers (below ~10%), the ASASP probe sees only a small fraction of the particles present (~2–20%), and consequently there is no significant correlation between ASASP count and CO concentration (Table 1) in these dry air masses. However, most of the plumes showed humidities above 25%, and here the correlation between ASASP particle count and CO are very high. It must also be emphasized, that the particles in the size range observed by the ASASP probe dominate the light scattering and cloud nucleation effects as well as the aerosol mass and are therefore the most important size class from the point of view of climate and atmospheric chemistry.

Unfortunately, there is little published data that the ob-

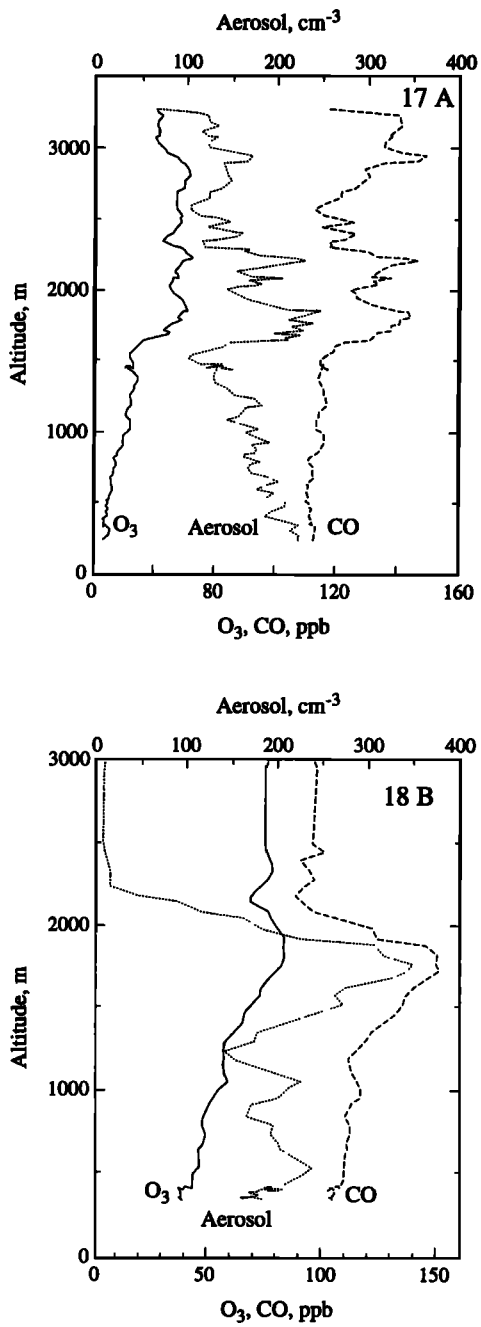

Figure 10. (continued)

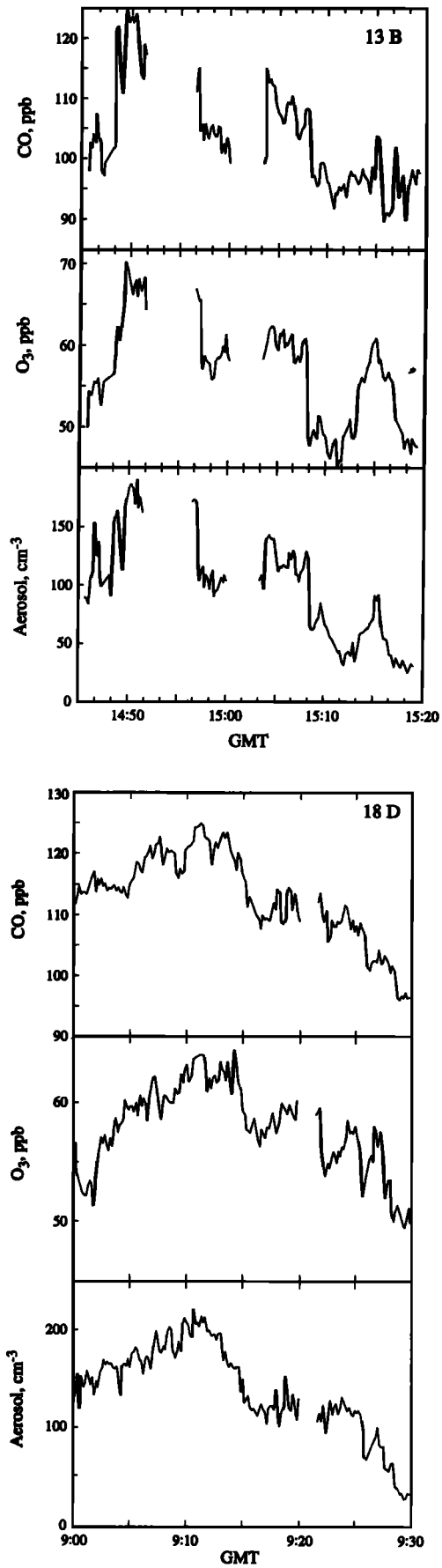

Figure 11. O_3, CO, and fine aerosol particle concentrations during level flight legs in haze layers (data from levels 13B and 18D).

served ratio $\Delta N_p/\Delta CO$ can be compared with. A direct comparison can only be made with the data from the first part of CITE 3, where *Anderson et al.* [1993a] found a mean $\Delta N_p/\Delta CO$ ratio of 7.7 cm^{-3} ppb^{-1} (range 2.6–12.5 cm^{-3} ppb^{-1}) in the North American plume. This agreement must be considered rather coincidental, however, since most of the particles in the North American plume are expected to be sulfate aerosol formed from the oxidation of SO_2 from fossil fuel burning. For the biomass burning plumes investigated during the DECAFE 88 expedition in the northern Congo [*Andreae et al.*, 1992], a $\Delta(CN)/\Delta CO$ of about 8–18 cm^{-3} ppb^{-1} can be calculated, significantly higher than the mean ratio from the CITE 3 ASASP data (5.2 ± 1.7). However, when the $\Delta N_p/\Delta CO$ ratios are corrected for the effect of relative humidity using the relationship between N_p/N_{CN}

Table 1. Regressions of Ozone, Aerosol Mass, and Aerosol Number Concentrations on CO Concentration for the Plumes Encountered During CITE 3

Plume ID	Type[a]	Altitude, m	Θ,[b] K	Air Mass Origin	RH,[c] %	Number of Data	Ozone			Aerosol Mass			Aerosol Number			
							$\Delta O_3/\Delta CO$	±	r^2	$\Delta M/\Delta CO$	±	r^2	$\Delta N/\Delta CO$	±	r^2	Humidity Adjusted
							Flight 12									
12C1	L	4000	320	W Afr	6.6	350	0.57	0.02	0.72		NC			NC		
12C2	L	4600	320	W Afr	6.4	137	0.68	0.03	0.76		NC			NC		
12D1	S	4200	318	W Afr	4.3	12	0.61	0.15	0.65		NC			NC		
12D2	S	2400	308	S Am	28	13	0.19	0.03	0.74	52.8	2.8	0.95	5.4	0.4	0.88	17.0
							Flight 13									
13AA	S	2100	310	S Atl	24	9	0.88	0.25	0.63	58.3	16.8	0.65	5.6	1.4	0.56	19.9
13B	L	2000	305	S Atl	45	188	0.68	0.04	0.64	45.4	1.5	0.79	6.0	0.2	0.82	12.4
13A	S	>1000	310–325	S Am	4	73	0.89	0.03	0.92		NC			NC		
13C1	S	3900	320	S Am	6.6	10	0.46	0.07	0.84		NC			NC		
13C2 +13D	S/L	2200	304	S Atl	45	69	0.42	0.03	0.71	44.1	2.9	0.69	4.5	0.2	0.78	9.4
							Flight 14									
14A1	S	2000	307	S Atl	37	26	0.15	0.02	0.77	27.4	1.9	0.84	3.9	0.2	0.88	9.6
14A2	S	1500	303	S Atl	50	17	0.48	0.08	0.71	36.6	1.2	0.32	4.6	0.7	0.69	8.8
14B/C	S/L	1600	305	S Atl	50	113	0.13	0.01	0.55	24.7	0.7	0.89	3.5	0.1	0.88	6.6
14D[4)]	S/L	1700	306	W Afr	35	...	0.20	...	...		...	...	3.1	...	...	8.1
							Flight 15									
15AA	S	1400	306	S Atl	28	33	0.71	0.07	0.70	38.6	5.0	0.58	3.5	0.5	0.54	11.0
15A		1600–2500		W Afr	40	47				23.2	0.3	0.97	3.7	0.2	0.84	8.5
15A1	S	1700	306	W Afr	49	11	0.12	0.02	0.91							
15A2	S	2200	309	W Afr	24	7	0.40	0.05	0.89							
15A3	L	1500	306	W Afr	35	113		NC		24.5	0.8	0.94	3.4	0.1	0.91	8.8
15B	S	1400	309	W Afr	48	17	0.24	0.04	0.88	34.1	0.2	0.92	4.3	0.3	0.91	8.5
							Flight 16									
16A	L	1500	303	S Atl	82	104	0.11	0.01	0.50	24.8	1.5	0.64	2.9	0.2	0.70	3.6
16B1	S	2500	310	S Afr	33	27	0.29	0.03	0.81	32.6	1.4	0.93	4.1	0.2	0.94	11.1
16B2	S	1900	306	S Atl	39	18	0.28	0.04	0.78	35.7	2.0	0.93	4.8	0.3	0.93	11.4
16B3	S	900	302	S Atl	64	17		NC		39.3	3.0	0.90	5.1	0.5	0.87	7.8
16C	S	2500	311	S Afr	52	36	0.78	0.06	0.82	29.4	2.2	0.70	4.0	0.3	0.75	7.2
16D1	S	2500	312	S Afr	41	45	0.76	0.06	0.77	37.0	1.9	0.82	4.1	0.3	0.79	9.4
16D2	S	900	302	S Atl	75	23	0.37	0.06	0.66	59.5	4.7	0.86	8.6	0.5	0.92	11.2
16	L	1500	303	S Atl	84	141	0.59	0.02	0.89	38.8	1.1	0.86	5.3	0.1	0.89	6.2
							Flight 17									
17A1	S	3100	311	S Afr	54	17	0.88	0.32	0.60	53.7	6.0	0.72	3.9	0.4	0.82	6.9
17A2	S	1600–2800	309	S Afr	52	45	0.45	0.03	0.86	35.4	3.1	0.64	5.6	0.2	0.90	10.3
17B	S	2500–3100	312	S Afr	32	26	0.20	0.01	0.91	31.0	1.8	0.86	3.9	0.3	0.83	10.9
17D	S	1900–3100	310	S Afr	31	32	0.21	0.02	0.85	32.7	3.5	0.63	5.5	0.3	0.86	16.0
							Flight 18									
18A1	S	1700	303	S Am	58	13	0.62	0.12	0.71		NC		6.4	0.4	0.97	10.6
18A2	S	1900	304	S Am	86	8		NC		280.7	57.0	0.71	15.2	3.0	0.74	17.5
18AB	L	3100	312	S Am/S Afr	12	84	0.20	0.03	0.33		NC			NC		
18B1	S	1900	305	S Atl	32	19	0.36	0.02	0.94	43.0	1.5	0.97	5.6	0.2	0.97	15.7
18B2	S	1200	302	S Am	74	8	0.62	0.08	0.91	72.1	11.3	0.84	10.6	1.1	0.92	14.1
18C1	S	1900	305	S Atl	73	17	0.50	0.09	0.66	31.4	3.9	0.71	5.0	0.6	0.72	6.8
18C2	S	2500	310	S Afr	20	17	0.78	0.10	0.82	28.9	0.9	0.98	4.4	0.2	0.97	18.3
18C3	S	3700	317	S Afr	7.3	12	2.43	0.35	0.83		NC			NC		
18D	L	1600	303	S Am	70	169	0.42	0.02	0.81	39.2	0.8	0.90	7.1	0.1	0.92	9.9
18	L	2800	311	S Am/S Afr	10	137		NC		18.8	0.6	0.81	3.2	0.2	0.58	22.1
18F	S	1900	308	S Atl	37	13	0.63	0.08	0.86	67.2	4.3	0.93	8.0	0.6	0.92	19.9

Table 1. (continued)

Plume ID	Type[a]	Altitude, m	Θ,[b] K	Air Mass Origin	RH,[c] %	Number of Data	Ozone ΔO3/ΔCO	±	r^2	Aerosol Mass ΔM/ΔCO	±	r^2	Aerosol Number ΔN/ΔCO	±	r^2	Humidity Adjusted
						Flight 19										
19A[d]	S	1700	306	S Am	31	...	0.52	...	...		...	...	6.8	...	...	19.7
19B	S	1600	306	S Am	28	16	0.27	0.04	0.79	55.5	1.9	0.98	7.0	0.4	0.95	22.2
19D	L	1600	306	S Am	26	133	0.54	0.02	0.82	35.8	1.1	0.85	5.8	0.2	0.89	19.5
190	L	2800	312	S Am	9.6	98	0.34	0.04	0.39		ND			ND		
19F	S	1200–2500	306–309	S Am	39	16	0.33	0.05	0.78	62.3	4.1	0.92	8.2	0.5	0.93	19.4
Average[e]							0.46			39.8			5.2			12.2
s.d.							0.23			13.3			1.7			5.0

CITE, Chemical Instrumentation Test and Evaluation; W Afr, West Africa; S Atl, South Atlantic; S Am, South America; S Afr, South Africa; NC, no correlation.

[a]L, level flight legs; S, spiral soundings.

[b]Potential temperature.

[c]Relative humidity.

[d]Slope derived from evaluation of analog data.

[e]Calculated without 18C3, aerosol mass slope also without 18A2.

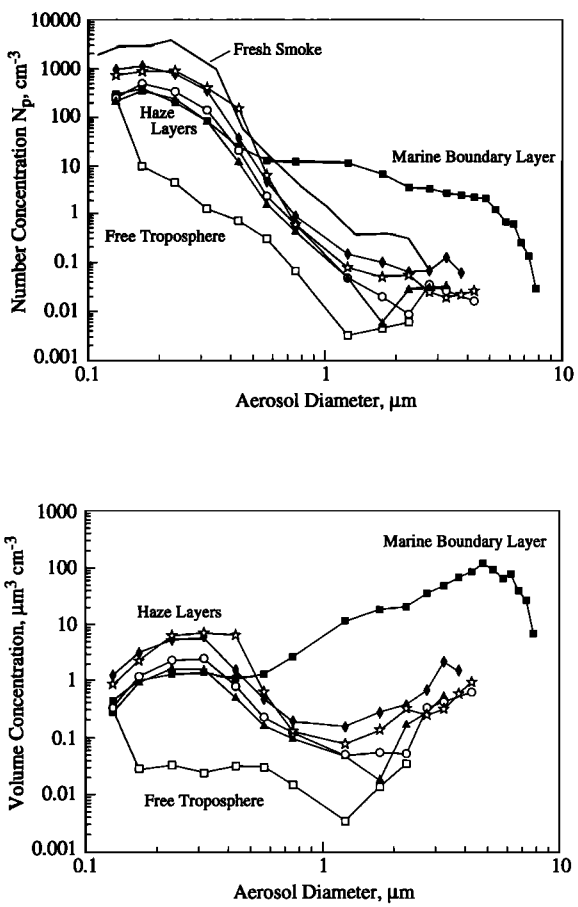

Figure 12. Aerosol size distributions from the haze layers (stars, flight 12 at 2000 m; circles, flight 15 at 1800 m; diamonds, flight 16 at 3000 m; triangles, flight 18 at 2600 m). For comparison a sample from the unpolluted marine boundary layer (closed squares, flight 11 at 150 m) and from the free troposphere away from the haze layers (open squares, flight 12 at 2100 m) are shown. Figure 12a shows the number distribution, 12b the volume distribution versus particle diameter. The number distribution from the fresh smoke of a savanna fire is indicated in Figure 12 (top) as a line without symbols.

ratio and relative humidity, a mean Δ(CN)/ΔCO ratio of 12.2 ± 5.0 is obtained, quite similar to the results from DECAFE 88.

From the particle number versus size distributions provided by the ASASP instrument, we have calculated the aerosol mass concentration. We assume a density of 1 g cm^{-3} for the aerosol particles, which is a reasonable approximation for particles consisting to a large degree of organic material. Densities near 1 g cm^{-3} were observed for smoke aerosol particles by *Stith et al.* [1981] and *Radke et al.* [1991]. Statistical analysis of the data obtained in the haze layers shows that the aerosol mass in the size fraction below 1 μm diameter is highly correlated with CO concentration (Table 1). The mean slope of submicron mass versus CO (i.e., the ratio ΔM(Aerosol)/ΔCO) is 40.0 ± 13.7 ng m^{-3} (STP) ppb^{-1} (n = 32). Total aerosol mass is not always well correlated with CO, since relatively small amounts of sea-salt aerosol can completely overwhelm the relatively modest mass concentrations present in the haze layers (typically 1–2 μg m^{-3} (STP), versus a (wet) sea-salt aerosol loading of 10–30 μg m^{-3} in the boundary layer). When sea-salt aerosol

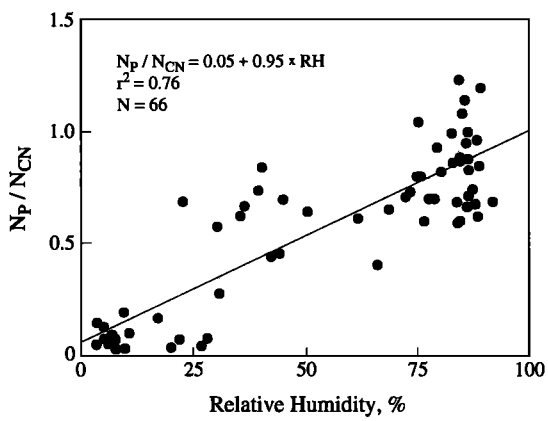

Figure 13. The ratio of particles >0.12 μm diameter over total particles, N_p/N_{CN}, as a function of relative humidity, RH.

Table 2. Nonmethane Hydrocarbons From Fire Plumes and From the Unpolluted Boundary Layer and Free Troposphere

Plume	Altitude, m	Ethane, ppb C	Ethylene,[a] ppb C	Acetylene, ppb C	Propane, ppb C	Propylene, ppb C	Butane, ppb C	Isobutane, ppb C	Sum,[b] ppb C
14B/C	1510	1.99	1.63	1.04	1.79	0.06	1.31	0.08	7.91
16E	1520	2.32	2.13	2.06	1.60	0.96	2.52	1.45	13.04
18D	1510	2.07	1.41	1.17	1.01	0.14	1.67	0.18	7.65
18E	2750	2.88	0.85	1.75	3.18	0.35	2.10	0.40	9.76
19D	1470	2.25	2.54	1.28	0.72	0.20	2.08	0.20	9.27
19E1	2750	2.99	3.58	1.31	0.81	0.51	2.11	0.47	11.78
					Plume				
Mean		2.42 ± 0.38	2.02 ± 0.88	1.44 ± 0.35	1.52 ± 0.84	0.37 ± 0.30	1.97 ± 0.38	0.46 ± 0.46	9.90 ± 1.95
					Boundary Layer				
Mean	<300	1.87 ± 0.38	1.32 ± 0.78	0.76 ± 0.23	1.19 ± 0.23	0.26 ± 0.13	1.38 ± 0.57	0.42 ± 0.15	6.38 ± 0.97
					Free Troposphere				
Mean	>3000	1.72 ± 0.06	0.74 ± 0.32	0.63 ± 0.06	0.77 ± 0.03	ND[c]	1.04 ± 0.08	0.45 ± 0.01	5.19 ± 0.53

[a]Peak also contains a fluorocarbon.
[b]Sum of all separated NMHC peaks.
[c]Not detectable.

is absent in the haze layers which are well separated from the boundary layer, most of the aerosol mass is in the submicron fraction, and the regression results become almost identical for total or submicron aerosol against CO. This is consistent with the aerosol size spectra observed in the plumes from CITE 3 and with literature data on the size distribution of aerosols from biomass fires [*Radke et al.*, 1978, 1988, 1991; *Stith et al.*, 1981; *Holben et al.*, 1991].

Our ΔM(aerosol)/ΔCO ratio of 40.0 ± 13.7 ng m^{-3} (STP) ppb^{-1} is considerably lower than the ratios calculated from most published emission factor data for particulate matter and CO [*Andreae et al.*, 1988; *Radke et al.*, 1991; *Susott et al.*, 1990; *Einfeld et al.*, 1991; *Ward et al.*, 1990, 1991; *Ward and Hardy*, 1986, 1991]. The literature ratios typically fall in the range from 90 to 180 ng m^{-3} (STP) ppb^{-1}. However, lower ratios have been reported, particularly from fires in the "cerrado," the Brazilian savannas, where *Ward et al.* [1992] obtained a mean ΔM(aerosol)/ΔCO ratio of 43.8 ± 17.5 ng m^{-3} (STP) ppb^{-1}. In smoke from deforestation fires this ratio was much higher, 101 ± 24 ng m^{-3} (STP) ppb^{-1}. Low aerosol emission factors from flaming-dominated savanna fires can thus probably account for much of the low ΔM(aerosol)/ΔCO ratios observed. However, it cannot be excluded that scavenging of as much as half of the aerosol mass during cloud cycling and precipitation may also account for some of the low ratios.

Nonmethane Hydrocarbons

Six of the hydrocarbon canister samples collected during CITE 3 were taken within plume layers. Unfortunately, they all missed the more concentrated parts of the plumes, and they contain relatively low concentrations of hydrocarbons. CO concentrations during the NMHC sampling times are only 10–40 ppb over the background values. Nevertheless, slight enrichment of a series of hydrocarbons relative to the unpolluted boundary layer and to the free troposphere above 3000-m altitude are evident (Table 2). The hydrocarbon distribution shows the acetylene, ethene, and ethane enrichment typical of pyrogenic emissions [*Greenberg et al.*, 1984; *Rudolph et al.*, 1992]. The alkenes are less enriched relative to the alkanes than in fresh smoke, consistent with an advanced plume age.

Nitrogen Oxides and Ozone Formation

The concentrations of NO, NO_2, and NO_y in the plumes are given in Table 3. Given the elevated concentrations of other pyrogenic pollutants in these plume layers, the concentrations of NO and NO_2 are quite low, 8 ± 6 and 37 ± 17 ppt, respectively. Clear correlations between pyrogenic tracer species and NO_x enrichments were not apparent. The low NO_x levels and the absence of correlations between NO_x and CO is probably due to the age of the plumes, in which most NO_x would have already reacted away within 1–2 days. The low ratio of NO to O_3 measured in most of the plumes suggests that ozone production has ceased, or that ozone may even be consumed in some cases.

In contrast, NO_y concentrations were high in most of the plume layers, and in spite of the limitations imposed by the time resolution of the NO_y data, correlations with other pyrogenic species could in several cases be obtained. Table 3 contains $\Delta NO_y/\Delta CO$ enhancement factors for these cases (average 0.053 ± 0.027). Since most of the NO_y in the plumes presumably originates from the conversion of NO_x emitted by the fires, this ratio provides an indication for the original emission ratio $\Delta NO_x/\Delta CO$. However, given the age of the CITE 3 plumes, the original ratio is difficult to deduce with certainty from the observed $\Delta NO_y/\Delta CO$ ratios. Assuming that some loss of NO_y has occurred due to aerosol formation and precipitation removal, these $\Delta NO_y/\Delta CO$ ratios would be consistent with initial $\Delta NO_x/\Delta CO$ of up to 0.1. Such high NO_x enrichments would explain the efficient ozone formation observed [*Jacob et al.*, 1992].

In general, our $\Delta NO_y/\Delta CO$ values are substantially larger than most of the values previously reported from forest burning [*Andreae*, 1993a, and references therein], e.g., those found for smoldering tundra fires in the subarctic (0.006 ± 0.006 [*Wofsy et al.*, 1992]) and deforestation fires in Amazonia (0.016 [*Andreae et al.*, 1988]). They are also at the high end of the range of values found in boreal/taiga fire plumes during ABLE 3A and ABLE 3B: $\Delta NO_y/\Delta CO \approx 0.02$–$0.04$

Table 3. Nitrogen Oxide Concentration and NO_y and O_3 Enrichment Ratio in the Plumes

Plume ID	NO		NO_2		NO_y		$\Delta NO_y/\Delta CO$	$\Delta O_3/\Delta CO$
	Mean	s.d.	Mean	s.d.	Mean	s.d.		
12C1	21	5	44	12	1150	300		
12C2	13	6	44	12	1910	270		
12D2	4	2	64	11	9240	170	0.020	0.19
13B	5	3	25	5	1360	160		
13A	23	5	37	9	420	30		
13D	5	2	24	5	2860	60		
14B/C	7	2	ND	ND	7860	1290		
14D/E	11	5	ND	ND	2810	1160		
15A	3	0	46	10	2810	570		
15A3	3	0	40	6	2040	420		
15B	3	1	42	10	3270	80	0.022	0.24
16A	3	1	47	10	11580	3270		
16B1	13	3	70	11	7920	100	0.052	0.29
16B2	11	3	56	10	9850	100	0.063	0.28
16B3	6	0	34	19	11450	650		
16C	14	3	79	11	3990	60		
16D1	9	5	52	24	4360	560		
16D2	3	1	23	10	5250	90		
16E	3	1	24	6	4290	460		
17A1	4	2	48	8	4610	70	0.064	0.87
17A2	4	0	40	2	5090	870	0.067	0.45
17B	4	1	38	10	2130	610		
18B	5	0	26	3	5250	1380	0.035	0.36
18C1	3	2	24	8	2280	70	0.077	0.50
18C2	11	3	51	10	960	40		
18C3	17	4	51	11	1590	50		
18D	6	2	21	7	2460	190		
18E	14	2	46	9	1110	100		
18F	5	2	25	11	8340	160	0.107	0.63
19B	8	3	12	6	6990	90	0.018	0.27
19D	15	5	36	8	1810	360		
19E1	15	2	46	9	1060	80		
19F	9	3	32	12	6770	100		
Mean	8		38		4390		0.053	0.41
s.d.	6		17		3146		0.027	0.20

Concentrations in ppt.

[*Sandholm et al.*, 1992, 1994]. On the other hand, the $\Delta NO_y/\Delta CO$ enhancement factors in Table 3 are close to fresh plume emission factors for chaparral fires in southern California: 0.04–0.24 [*Laursen et al.*, 1992]. Unfortunately, there are few NO_x emission factors for savanna fires available in the literature. Over savanna fires in the Ivory Coast, *Lacaux et al.* [1993] measured a $\Delta NO_x/\Delta CO$ ratio of 0.022 and a $\Delta NO_y/\Delta CO$ ratio of 0.031. However, it can be expected that savanna fires will generally produce relatively high $\Delta NO_x/\Delta CO$ ratio, since this ratio depends strongly on the prevailing type of combustion. Only in flaming combustion is a significant amount of the fuel nitrogen converted to NO_x, whereas the production of CO, CH_4, and NMHC occurs predominantly in smoldering combustion [*Kuhlbusch et al.*, 1991; *Lobert et al.*, 1990, 1991]. The emission ratio $\Delta NO_x/\Delta CO_2$ has been shown to be almost universally constant at about $2 \pm 1 \times 10^{-3}$ in a wide variety of fires worldwide [*Crutzen et al.*, 1985; *Andreae et al.*, 1988; *Lobert et al.*, 1991; *Laursen et al.*, 1992; *Lacaux et al.*, 1993; *Helas et al.*, 1994]. On the other hand, the emission ratios $\Delta CO/\Delta CO_2$ and $\Delta NMHC/\Delta CO_2$ are about 2–4 times higher in forest fires, which have a substantial smoldering component, than in savanna fires, which are dominated by flaming combustion [*Ward et al.*, 1991; *Helas et al.*, 1994]. As a result, emissions from savanna fires, which are the most likely source of the plumes investigated during CITE 3, have higher $\Delta NO_x/\Delta CO$ and $NO_x/NMHC$ ratios than emissions from cooler fires, such as the deforestation fires which produced the smoke plumes observed over Amazonia by *Andreae et al.* [1988] and over the Arctic tundra by *Wofsy et al.* [1992]. For example, in smoke plumes from savanna fires in Brazil, *Ward et al.* [1991] found a $\Delta CO/\Delta CO_2$ ratio of only 0.022, which when combined with an average NO_x emission ratio of 0.0021 yields a $\Delta NO_x/\Delta CO$ emission ratio of about 0.1. Similar emission ratios for CO and NO_x were recently observed over savanna fires in southern Africa (G. Helas, personal communication, 1993). It appears that savanna fires have $\Delta NO_x/\Delta CO$ ratios similar to urban values, which lie around 0.03–0.05, for example, in the case of New York City [*Wofsy et al.*, 1992]. This would be consistent with the high ozone production efficiency observed in the CITE 3 plumes. Indeed, the ozone production efficiency, expressed by the ratio $\Delta O_3/\Delta CO$, increases with increasing $\Delta NO_y/\Delta CO$ in the plumes (Figure 14).

Around September, savanna burning in southern Africa, cerrado (savanna) fires in Brazil, and grassland fires in the pampas of South America reach their seasonal maxima [*Kirchhoff and Rasmussen*, 1990; *Andreae*, 1993b]. Given the observation that most of the air mass trajectories reach back into savanna areas on the continents on either side of

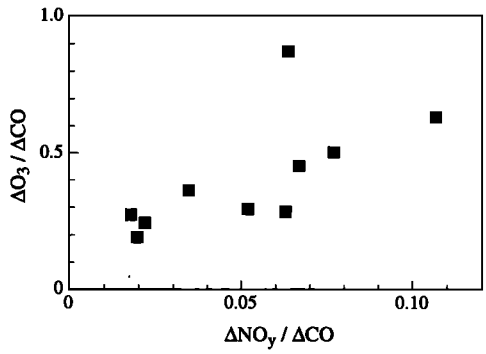

Figure 14. The ozone production ratio, $\Delta O_3/\Delta CO$, versus the $\Delta NO_y/\Delta CO$ ratio measured in the plumes.

the Atlantic, and the large areas burned every year in these regions, it is plausible that the high ratios of $\Delta NO_y/\Delta CO$ and, consequently, of $\Delta O_3/\Delta CO$ observed during CITE 3 result from the flaming-dominated mode of combustion in savannas.

Overview and Conclusion

The preceding discussion has shown that a number of atmospheric species which originate in biomass burning (carbon monoxide, nonmethane hydrocarbons, oxides of nitrogen, and smoke aerosol particles) were present over a large fraction of the area investigated during CITE 3. The analysis of air mass trajectories and streamline charts points to savanna and grassland fires, predominantly in Africa but also in South America, as the source of these pyrogenic species. As a result of photochemical reactions during the prolonged transport of these smoke-laden air masses, substantial amounts of ozone are formed, resulting in a considerable enrichment of ozone in the troposphere.

In the same region, satellite analyses have shown an enhancement of tropospheric ozone by about 15–20 Dobson units (DU) over the tropical background value during the September–October period [*Fishman et al.*, 1991]. From a statistical analysis of the O_3 data collected during CITE 3, *Anderson et al.* [1993b] derive an average ozone column concentration of 13.5 DU in the lower troposphere (up to 3.3 km, the maximum altitude for most flights). Based on a comparison with wet season data, they deduce that during CITE 3, ozone in this layer was enhanced by about 8–9 DU over the average wet season value and that about 50% of this enhancement can be attributed to ozone formation from pyrogenic precursors. Clearly, this photochemical ozone source and the resulting plumes in the lower troposphere alone cannot explain the 15–20-DU ozone enrichment observed by remote sensing.

Ozone sondes launched during CITE 3 showed that elevated O_3 levels were present throughout the troposphere, resulting in a tropospheric ozone column of 39–51 DU, in good agreement with the satellite results of *Fishman et al.* [1991]. Since no pyrogenic tracers are available to establish the source of these ozone enriched layers (photochemical production or downward mixing from the stratosphere), the role of biomass burning in the formation of the ozone maximum over the South Atlantic cannot be determined on the basis of the results from CITE 3. Recent work during the 1992 STARE (Southern Tropical Atlantic Regional Experiment), consisting of the two components TRACE A (Transport and Atmospheric Chemistry near the Equator, Atlantic) and SAFARI (Southern Africa Fire/Atmosphere Research Initiative), showed that smoke plumes containing high amounts of ozone, aerosols, and carbon monoxide were indeed present throughout the troposphere in the South Atlantic region (J. Fishman et al., personal communication, 1993). These results suggest that photochemical ozone production in the smoke plumes emitted from the vast areas of savannas and tropical forest, which are subjected to burning every year, represents a major source of ozone to the tropical troposphere. Furthermore, the smoke aerosol particles contained in these plumes may make a significant contribution to the radiative properties of the atmosphere in the tropics and to the concentrations of cloud condensation nuclei (CCN). The perturbation of the radiation budget due to aerosol backscatter and due to the modification of cloud albedo by increased CCN concentrations may have a considerable effect on regional and global climate [*Penner et al.*, 1991, 1992; *Andreae*, 1994].

Acknowledgments. We acknowledge the permission of the Government of Brazil to conduct this research in Brazil. The cooperation of the flight crew of the NASA Electra research aircraft is gratefully acknowledged. Thanks are due to I. Bambach for help with the production of the figures. This research was supported by the Max Planck Society and by the NASA Tropospheric Chemistry Program.

References

Anderson, B. E., G. L. Gregory, J. D. W. Barrick, J. E. Collins, G. W. Sachse, D. Bagwell, M. Shipham, J. D. Bradshaw, and S. T. Sandholm, The impact of U.S. continental outflow on ozone and aerosol distributions over the western Atlantic, *J. Geophys. Res.*, *98*, 23,477–23,489, 1993a.

Anderson, B. E., G. L. Gregory, J. D. W. Barrick, J. E. Collins, G. W. Sachse, C. H. Hudgins, J. D. Bradshaw, and S. T. Sandholm, Factors influencing dry season ozone distributions over the tropical South Atlantic, *J. Geophys. Res.*, *98*, 23,491–23,500, 1993b.

Andreae, M. O., The influence of tropical biomass burning on climate and the atmospheric environment, in *Biogeochemistry of Global Change: Radiatively Active Trace Gases*, edited by R. S. Oremland, pp. 113–150, Chapman and Hall, New York, 1993a.

Andreae, M. O., Global distribution of fires seen from space, *Eos Trans. AGU*, *74*, 129, 135, 1993b.

Andreae, M. O., Climatic effects of changing atmospheric aerosol levels, in *World Survey of Climatology*, vol. 16, *Future Climates of the World*, edited by A. Henderson-Sellers, Elsevier, New York, in press, 1994.

Andreae, M. O., et al., Biomass-burning emissions and associated haze layers over Amazonia, *J. Geophys. Res.*, *93*, 1509–1527, 1988.

Andreae, M. O., A. Chapuis, B. Cros, J. Fontan, G. Helas, C. Justice, Y. J. Kaufman, A. Minga, and D. Nganga, Ozone and Aitken nuclei over equatorial Africa: Airborne observations during DECAFE 88, *J. Geophys. Res.*, *97*, 6137–6148, 1992.

Blake, D. R., D. F. Hurst, T. W. Smith Jr., W. J. Whipple, T.-Y. Chen, N. J. Blake, and F. S. Rowland, Summertime measurements of selected nonmethane hydrocarbons in the Arctic and subarctic during the 1988 Arctic Boundary Layer Expedition (ABLE 3A), *J. Geophys. Res.*, *97*, 16,559–16,588, 1992.

Bradshaw, J. D., M. O. Rodgers, S. T. Sandholm, S. KeSheng, and D. D. Davis, A two-photon laser-induced fluorescence field instrument for ground-based and airborne measurements of atmospheric NO, *J. Geophys. Res.*, *90*, 12,861–12,877, 1985.

Chatfield, R. B., and A. C. Delany, Convection links biomass burning to increased tropical ozone: However, models will tend to overpredict O_3, *J. Geophys. Res.*, *95*, 18,473–18,488, 1990.

Cros, B., D. Nganga, A. Minga, J. Fishman, and V. Brackett, Distribution of tropospheric ozone at Brazzaville, Congo, deter-

mined from ozonesonde measurements, *J. Geophys. Res.*, *97*, 12,869–12,875, 1992.

Crutzen, P. J., A. C. Delany, J. P. Greenberg, P. Haagenson, L. Heidt, R. Lueb, W. Pollock, W. Seiler, A. F. Wartburg, and P. R. Zimmerman, Tropospheric chemical composition measurements in Brazil during the dry season, *J. Atmos. Chem.*, *2*, 233–256, 1985.

Danielsen, E. F., Trajectories: Isobaric, isentropic, and actual, *J. Meteorol.*, *18*, 479–486, 1961.

Einfeld, W., D. E. Ward, and C. C. Hardy, Effects of fire behavior on prescribed fire smoke characteristics: A case study, in *Global Biomass Burning: Atmospheric, Climatic, and Biospheric Implications*, edited by J. S. Levine, pp. 412–419, MIT Press, Cambridge, Mass., 1991.

Fishman, J., and J. C. Larsen, The distribution of total ozone and stratospheric ozone in the tropics: Implications for the distribution of tropospheric ozone, *J. Geophys. Res.*, *92*, 6627–6634, 1987.

Fishman, J., C. E. Watson, J. C. Larsen, and J. A. Logan, Distribution of tropospheric ozone determined from satellite data, *J. Geophys. Res.*, *95*, 3599–3617, 1990.

Fishman, J., K. Fakhruzzaman, B. Cros, and D. Nganga, Identification of widespread pollution in the southern hemisphere deduced from satellite analyses, *Science*, *252*, 1693–1696, 1991.

Greenberg, J. P., P. R. Zimmerman, L. Heidt, and W. Pollock, Hydrocarbon and carbon monoxide emissions from biomass burning in Brazil, *J. Geophys. Res.*, *89*, 1350–1354, 1984.

Gregory, G. L., C. H. Hudgins, and R. A. Edahl Jr., Laboratory evaluation of an airborne ozone instrument which compensates for altitude/sensitivity effects, *Environ. Sci. Technol.*, *17*, 100–103, 1983.

Gregory, G. L., E. V. Browell, and L. S. Warren, Boundary layer ozone: An airborne survey above the Amazon basin, *J. Geophys. Res.*, *93*, 1452–1468, 1988.

Haagensen, P. L., and M. A. Shapiro, Isentropic trajectories for derivation of objectively analyzed meteorological parameters, *Tech. Note NCAR/TN-149*, 30 pp., Natl. Cent. for Atmos. Res., Boulder, Colo., 1979.

Helas, G., et al., Airborne measurements of savanna fire emissions and the regional distribution of pyrogenic pollutants over western Africa, *J. Atmos. Chem.*, in press, 1994.

Hoell, J. M. Jr., et al., Operational overview of the NASA GTE/CITE 3 airborne instrument intercomparisons for sulfur dioxide, hydrogen sulfide, carbonyl sulfide, dimethyl sulfide, and carbon disulfide, *J. Geophys. Res.*, *98*, 23,291–23,304, 1993.

Holben, B. N., Y. J. Kaufman, A. W. Setzer, D. D. Tanre, and D. E. Ward, Optical properties of aerosol emissions from biomass burning in the tropics, BASE-A, in *Global Biomass Burning: Atmospheric, Climatic, and Biospheric Implications*, edited by J. S. Levine, pp. 403–411, MIT Press, Cambridge, Mass., 1991.

Jacob, D. J., et al., Summertime photochemistry of the troposphere at high northern latitudes, *J. Geophys. Res.*, *97*, 16,421–16,431, 1992.

Kaufman, Y. J., A. Setzer, D. Ward, D. Tanre, B. N. Holben, P. Menzel, M. C. Pereira, and R. Rasmussen, Biomass Burning Airborne and Spaceborne Experiment in the Amazonas (BASE A), *J. Geophys. Res.*, *97*, 14,581–14,599, 1992.

Kirchhoff, V. W. J. H., and C. A. Nobre, Atmospheric chemistry research in Brazil: Ozone measurements at Natal, Manaus, and Cuiabá, *Rev. Geofis.*, *24*, 95–108, 1986.

Kirchhoff, V. W. J. H., and R. A. Rasmussen, Time variations of CO and O_3 concentrations in a region subject to biomass burning, *J. Geophys. Res.*, *95*, 7521–7532, 1990.

Kirchhoff, V. W. J. H., A. W. Setzer, and M. C. Pereira, Biomass burning in Amazonia: Seasonal effects on atmospheric O_3 and CO, *Geophys. Res. Lett.*, *16*, 469–472, 1989.

Kirchhoff, V. W. J. H., I. M. O. daSilva, and E. V. Browell, Ozone measurements in Amazonia: Dry season versus wet season, *J. Geophys. Res.*, *95*, 16,913–16,926, 1990.

Kirchhoff, V. W. J. H., R. A. Barnes, and A. L. Torres, Ozone climatology at Natal, Brazil, from in situ ozonesonde data, *J. Geophys. Res.*, *96*, 10,899–10,909, 1991.

Kuhlbusch, T. A., J. M. Lobert, P. J. Crutzen, and P. Warneck, Molecular nitrogen emissions from denitrification during biomass burning, *Nature*, *351*, 135–137, 1991.

Lacaux, J. P., J. M. Brustet, R. Delmas, J. C. Menaut, L. Abbadie, B. Bonsang, H. Cachier, J. Baudet, M. O. Andreae, and G. Helas, Biomass burning in the tropical savannas of Ivory Coast: An overview of the field experiment Fire of Savannas (FOS/DECAFE 91), *J. Atmos. Chem.*, in press, 1993.

Laursen, K. K., P. V. Hobbs, L. F. Radke, and R. A. Rasmussen, Some trace gas emissions from North American biomass fires with an assessment of regional and global fluxes from biomass burning, *J. Geophys. Res.*, *97*, 20,687–20,701, 1992.

Lobert, J. M., D. H. Scharffe, W.-M. Hao, and P. J. Crutzen, Importance of biomass burning in the atmospheric budgets of nitrogen-containing gases, *Nature*, *346*, 552–554, 1990.

Lobert, J. M., D. H. Scharffe, W. M. Hao, T. A. Kuhlbusch, R. Seuwen, P. Warneck, and P. J. Crutzen, Experimental evaluation of biomass burning emissions: Nitrogen and carbon containing compounds, in *Global Biomass Burning: Atmospheric, Climatic, and Biospheric Implications*, edited by J. S. Levine, pp. 289–304, MIT Press, Cambridge, Mass., 1991.

Marenco, A., J. C. Medale, and S. Prieur, Study of tropospheric ozone in the tropical belt (Africa, America) from STRATOZ and TROPOZ campaigns, *Atmos. Environ., Part A*, *24*, 2823–2834, 1990.

Penner, J. E., S. J. Ghan, and J. J. Walton, The role of biomass burning in the budget and cycle of carbonaceous soot aerosols and their climate impact, in *Global Biomass Burning: Atmospheric, Climatic and Biospheric Implications*, edited by J. S. Levine, pp. 387–393, MIT Press, Cambridge, Mass., 1991.

Penner, J. E., R. E. Dickinson, and C. A. O'Neill, Effects of aerosol from biomass burning on the global radiation budget, *Science*, *256*, 1432–1434, 1992.

Radke, L. F., J. L. Stith, D. A. Hegg, and P. V. Hobbs, Airborne studies of particles and gases from forest fires, *JAPCA*, *28*, 30–34, 1978.

Radke, L. F., D. A. Hegg, J. H. Lyons, C. A. Brock, P. V. Hobbs, R. Weiss, and R. Rasmussen, Airborne measurements on smokes from biomass burning in *Aerosols and Climate*, edited by P. V. Hobbs and M. P. McCormick, pp. 411–422, A. Deepak, Hampton, Va., 1988.

Radke, L. F., D. A. Hegg, P. V. Hobbs, J. D. Nance, J. H. Lyons, K. K. Laursen, R. E. Weiss, P. J. Riggan, and D. E. Ward, Particulate and trace gas emissions from large biomass fires in North America, in *Global Biomass Burning: Atmospheric, Climatic and Biospheric Implications*, edited by J. S. Levine, pp. 209–224, MIT Press, Cambridge, Mass., 1991.

Reichle, H. G. Jr., V. S. Conners, J. A. Holland, W. D. Hypes, H. A. Wallio, J. C. Casas, B. B. Gormsen, M. S. Saylor, and W. D. Hasketh, Middle and upper tropospheric carbon monoxide mixing ratios as measured by a satellite-borne remote sensor during November 1981, *J. Geophys. Res.*, *91*, 10,865–10,888, 1986.

Reichle, H. G. Jr., V. S. Connors, J. A. Holland, R. T. Sherrill, H. A. Wallio, J. C. Casas, E. P. Condon, B. B. Gormsen, and W. Seiler, The distribution of middle tropospheric carbon monoxide during early October 1984, *J. Geophys. Res.*, *95*, 9845–9856, 1990.

Rudolph, J., A. Khedim, and B. Bonsang, Light hydrocarbons in the tropospheric boundary layer over tropical Africa, *J. Geophys. Res.*, *97*, 6181–6186, 1992.

Sachse, G. W., R. C. Harriss, J. Fishman, G. F. Hill, and D. R. Cahoon, Carbon monoxide over the Amazon basin during the 1985 dry season, *J. Geophys. Res.*, *93*, 1422–1430, 1988.

Sandholm, S. T., J. D. Bradshaw, K. S. Dorris, M. O. Rodgers, and D. D. Davis, An airborne compatible photofragmentation two-photon laser-induced fluorescence instrument for measuring background tropospheric levels of NO, NO_x, and NO_2, *J. Geophys. Res.*, *95*, 10,155–10,161, 1990.

Sandholm, S. T., et al., Summertime tropospheric observations related to N_xO_y distributions and partitioning over Alaska: Arctic Boundary Layer Expedition 3A, *J. Geophys. Res.*, *97*, 16,481–16,509, 1992.

Sandholm, S. T., et al., Summertime partitioning and budget of NO_y compounds in the troposphere over Alaska and Canada: ABLE 3, *J. Geophys. Res.*, *99*, 1837–1861, 1994.

Shipham, M. C., A. S. Bachmeier, and B. E. Anderson, CITE 3 meteorological highlights, *J. Geophys. Res.*, *98*, 23,305–23,324, 1993.

Stith, J. L., L. F. Radke, and P. V. Hobbs, Particle emissions and

the production of ozone and nitrogen oxides from the burning of forest slash, *Atmos. Environ.*, *15*, 73–82, 1981.

Susott, R. A., D. E. Ward, R. E. Babbitt, D. J. Latham, L. G. Weger, and P. M. Boyd, Fire dynamics and chemistry of large fires, final report, 39 pp., U.S. Dep. of Agric. Forest Serv., Missoula, Mont., 1990.

Ward, D. E., and C. C. Hardy, Advances in the characterization and control of emissions from prescribed broadcast fires of coniferous species logging slash on clear-cut units, final report, U.S. Environmental Protection Agency and U.S. Department of Energy, Missoula, Mont., 1986.

Ward, D. E., and C. C. Hardy, Smoke emissions from wildland fires, *Environ. Int.*, *17*, 117–134, 1991.

Ward, D. E., R. A. Susott, R. E. Babbitt, and C. C. Hardy, Properties and concentration of smoke near the ground from biomass field tests, paper presented at the Symposium on Smoke/Obscurants XIV, Laurel, Md., April 17–19, 1990.

Ward, D. E., A. W. Setzer, Y. J. Kaufman, and R. A. Rasmussen, Characteristics of smoke emissions from biomass fires of the Amazon region—BASE A experiment, in *Global Biomass Burning: Atmospheric, Climatic, and Biospheric Implications*, edited by J. S. Levine, pp. 394–402, MIT Press, Cambridge, Mass., 1991.

Ward, D. E., R. A. Susott, J. B. Kauffman, R. E. Babbitt, D. L. Cummings, B. Dias, B. N. Holben, Y. J. Kaufman, R. A. Rasmussen, and A. W. Setzer, Smoke and fire characteristics for cerrado and deforestation burns in Brazil: BASE B experiment, *J. Geophys. Res.*, *97*, 14,601–14,619, 1992.

Watson, C. E., J. Fishman, and H. G. Reichle Jr., The significance of biomass burning as a source of carbon monoxide and ozone in the southern hemisphere tropics: A satellite analysis, *J. Geophys. Res.*, *95*, 16,443–14,450, 1990.

Wofsy, S. C., et al., Atmospheric chemistry in the Arctic and subarctic: Influence of natural fires, industrial emissions, and stratospheric inputs, *J. Geophys. Res.*, *97*, 16,731–16,746, 1992.

B. E. Anderson, J. E. Collins, G. L. Gregory, G. W. Sachse, and M. C. Shipham, NASA Langley Research Center, Atmospheric Sciences Division, Hampton, VA 23681-0001.

M. O. Andreae, Max Planck Institute for Chemistry, Biogeochemistry Department, P. O. Box 3060, D-55020 Mainz, Germany.

D. R. Blake, Department of Chemistry, University of California, Irvine, CA 92717.

J. D. Bradshaw, Georgia Institute of Technology, School of Geophysical Sciences, Atlanta, GA 30332.

(Received August 17, 1993; revised December 16, 1993; accepted January 25, 1994.)